Nanoscale Thermal Transport Model of Magnetic Tunnel Junction (MTJ) device for STT-MRAM

Shaomin Li, Yanfeng Jiang

Department of Electrical Engineering, School of Internet of Things (IoTs), Jiangnan University, Wuxi, 214000, China

Spin-transfer-torque magnetic random access memory (STT-MRAM) based on magnetic tunnel junction (MTJ) device has attracted significant attentions from academics and industries. Nevertheless, the thermal effect under bias operation affects the overall performance and stability of the device. To evaluate the thermal phenomenon in MTJ device accurately, the non-equilibrium effect between the electron and the phonon near the electrode-barrier interface cannot be ignored. The existence of the interface leads to additional thermal resistance hindering the heat conduction of tunnel junction. Therefore, an effective equivalent model concerning the interface effect is necessary to represent the heat transportation of the device. In the paper, a nanoscale thermal transport model of the MTJ device is proposed. The influence of the thermal conductivity of the nano-oxide layer on the temperature distribution is discussed. The interface energy balance transport model is used to clarify the non-equilibrium relationship between the phonon and the electron at the CoFeB/MgO/CoFeB interfaces. A parameterization study is conducted to illustrate the temperature distribution in the nanoscale thermal transport model. Furthermore, the phonon-electron coupling distance (δ) based on the thermal conductivity of the phonon (κ_p) and the electron (κ_e) of the device is implemented to construct the effective equivalent model using finite element modeling (FEM), which could realistically reflect the thermal transport under working conditions. The established equivalent model has a guiding role in exploring the thermal transportation in the nanoscale MTJ device.

***Index Terms*—magnetic tunnel junction, thermal transport model, phonon-electron coupling, heat conductivity.**

I. INTRODUCTION

Spin-transfer-torque magnetic random-access-memory (STT-MRAM) is a novel non-volatile magnetic random access memory, which is regarded as one of the most potential candidates for next-generation memory due to its competitive performance characteristics, such as high write/read speed, unlimited endurance, and low energy consumption[1]. Moreover, the simple vertical structure is highly compatible with CMOS chip manufacturing process. The main component of the STT-MRAM memory cell is magnetic tunnel junction (MTJ), which is stacked on CMOS device by additional mask and deposition technologies to enable high memory densities [2]. Generally, the MTJ device is composed of two ferromagnetic layers with different thicknesses and a non-magnetic isolation layer with nanoscale thickness.

With the size of the memory cell keeps decreasing, the writing process of STT-MRAM is shown to be highly sensitive to Joule heating caused by electric spin current [3]. The heat transportation in the MTJ device promotes the coupling effect among the heat flux, the charge and the spin electron, thereby extending the complexity of the analysis on the spintronic device operation mechanism. For example, magnetothermoelectric phenomena is triggered by the tunnel magneto-seebeck (TMS) effect, which occurs in MTJ device because of the obvious thermal gradient across the barrier [4]. Also, the thermal spin-transfer torque induced by the heat transportation shows influence on the magnetic switching property [5]. Meanwhile, the self-heating problem, aroused by the heat flowing through the stacking of the multilayer, seriously affects the reliability of the device [6]. Based on the above mentioned thermal issues in the MTJ device, it is necessary to explore the characteristics of the heat transportation in the tunneling device.

The discussion on the internal heat transportation in STT-MRAM with nano-magnetic structure is mainly concentrated in the MTJ device. In the multi-layer stacking structure of the MTJ device, the interface conduction between different layers usually plays a pivotal role in the heat transportation. There are different types of interfaces in terms of the layer's thermal conductivity. The interface thermal resistance between two metal layers doesn't show obvious influence on the thermal conductivity [7]. On the contrary, when the interface is composed by the metal-oxide barrier, the heat is mainly transported by the phonon, which is mainly responsible for the heat transfer of the whole stack. However, when the size of the device is reduced to the nanoscale, the thermal conductivity of the oxide layer is decreased by several magnitude compared to the bulk ones. The degradation of the thermal conductivity has influence on the heat transfer mechanism in the device [8]. Moreover, the coupling between the electron and the phonon can't be neglected in the nano-device [9]. The imbalance of the thermal transportation by the electron and phonon at the metal-oxide interface would cause additional thermal resistance at the interface, which hinders the heat conduction of the tunnel junction.

Currently, the temperature distribution inside the nanoscale device is difficult to be measured experimentally [10]. Generally, the overall temperature variation of the MTJ device and the thermal gradient among the stacked layers can be estimated by solving the heat transfer equation with the finite

Manuscript received Month xx, 2xxx; revised Month xx, xxxx; accepted Month x, xxxx. This work was supported by NSFC (No.61774078). (Corresponding author:Yanfeng Jiang. E-mail: jiangyf@jiangnan.edu.cn)

S.M.Li, and Y.F.Jiang are with the Department of Electrical Engineering, Internet of Things Engineering College, Jiangnan University, WuXi 214122, China (E-mail:7191905003@stu.jiangnan.edu.cn; jiangyf@jiangnan.edu.cn)

This article has been accepted for publication in a future issue of this journal, but has not been fully edited. Content may change prior to final publication. Citation information: DOI 10.1109/TMAG.2022.3153363, IEEE Transactions on Magnetics

element modeling (FEM) approach [11]. However, the additional thermal resistance of the interface isn't included in the estimation. The ignorance causes obvious deviation from the actual situation, especially in spintronic nanoscale device, and should be addressed by considering the influence of the interface thermal resistance.

In the paper, the temperature distribution across the tunnel barrier is simulated by using FEM approach. The temperature distributions of the electron and the phonon are numerically characterized, revealing the imbalanced effect of the heat transportation at CoFeB/MgO/CoFeB interfaces. The quantified phonon-electron coupling non-equilibrium distance and the interface thermal resistance are included in the simulation to improve the accuracy of the temperature distribution predictions of the MTJ device.

II. Device And Simulation Details

A. Device Details

Fig. 1(a) shows the typical structure cell of STT-MRAM, including a transistor, a vertical MTJ device and the read-write electrodes. As the core cell, the MTJ device is composed of metal materials, ferromagnetic materials and oxide barrier layers with different thicknesses, which are deposited by radio frequency sputtering approach. The structure of the MTJ device is as follows from top to bottom: $Ta_{(20)}/Ru_{(5)}/Ta_{(5)}/CoFeB_{(5)}/Ta_{(5)}/CoFeB_{(5)}/MgO_{(2)}/CoFeB_{(5)}/Ru_{(5)}/Co_{(8)}/Pt_{(7)}/Ta_{(5)}/Ru_{(10)}/Ta_{(20)}/SiO_{2(50)}/Si_{(100)}$ (the thickness of the layer is marked in parenthesis in nm), which is shown in Fig. 1(b). In fact, the current is polarized when the current flows through the magnetic layers, forming a spin-polarized current. By changing the direction of the spin current, the magnetization moment of the free layer is reversed, resulting in parallel (P) or antiparallel (AP) states relative to the magnetization moment of the pinned layer as shown in Fig. 1(c). In the P state with low resistance, the information '0' can be stored. On the contrary, the information '1' is stored.

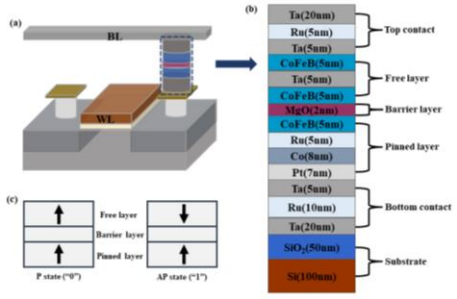

Fig. 1. (a) The typical structure cell of STT-MRAM. (b) The vertical stack structure of the MTJ device, including thickness details. (c) The fundamental working mechanism of the MTJ device.

B. Simulation Details

The FEM simulation is conducted to investigate the electro-thermal behavior. A multiphysics 2D-modeling coupled with solid heat transfer and circuit modules is established. The basic governing equation of heat transportation is given as [10]:

$$\rho C_p dT / dt + \nabla \cdot q = J \cdot E + Q \quad (1a)$$

$$J = \sigma E \quad (1b)$$

where ρ the mass density (kg/m^3), C_p the heat capacity (J/kg.K), T the temperature, t the time, q the heat flux vector that depends on the thermal conductivity κ (W/m.K) and the thermal gradient ∇T ($q = -\kappa \nabla T$), J the current density, σ the electrical conductivity, E the electric field and Q the heat generated on MTJ device by the self-heating effect (W/m^3).

In the simulation, the model geometry structure used for the simulation is simplified with layer thickness in nm as shown in Fig. 2(a) and the pivotal material parameters are shown in Table I. The parameters are referenced from [12,13]. The external circuit is applied as an additional heat source to the upper and lower electrodes of the MTJ device, with the positive direction representing the P state and the reverse direction representing the AP state. The dependence of the TMR on bias voltage is not considered in the model. The applied voltage amplitude and the pulse width have good consistency with the MTJ device under working condition. The voltage pulse signals with a continuous increasing of the amplitude from 0 to 1.5 V are applied on the model. Fig. 2(b) shows the schematic of the voltage pulses with the amplitude of 1.5 V. The heating period of the applied voltage is implemented to observe the self-heating effect of the MTJ device, and the cooling period is used to explore the transportation mechanism of the thermal gradient in the device, which is the main research progress of this article. The extracted temperature distribution between different film layers along the z direction is contributed for further exploration of the transmission mechanism of temperature across the interface. The initial temperature is set to be 300 K. The actual heat dissipation of the MTJ device in the integrated device is taken into account in the model. The boundary heat flux condition is set to be the external natural convection during the FEM simulation, and the external temperature is set to be 300 K. In addition, in order to visually evaluate the thermal diffusion gradient, a grid system is designed between the top contact and the bottom contact, allowing the heat to be diffused perpendicularly to the surface of the stacked structure.

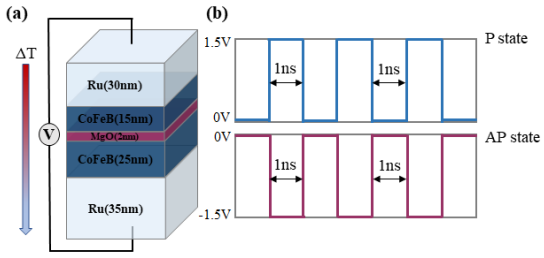

Fig. 2. (a) Simplified model structure for the heat transportation simulation, including geometric parameters in the model. (b) The schematic of the voltage pulses applied in P and AP state. The pulse amplitude is 1.5 V and the pulse width is set to be 1 ns.

TABLE I
PHYSICAL PARAMETERS FOR HEAT TRANSPORTATION MODEL

Material	σ (S/m)	κ (W/m.K)	ρ (kg/m^3)	C_p (J/kg.K)
Ru	1.37e7	117	12370	238
MgO	89	0.4-4.8	3580	935
CoFeB	9.43e6	88	8220	440

III. Results And Discussion

A. Heat transportation model

Using the established model, the heat transfer mechanism under the working states of the device is simulated, and the results are shown in Fig. 3. Fig. 3(a) shows the relationship between the temperatures of the whole stack of the MTJ device and the layer thickness with the voltage pulse applied (which being the heating process). During the heating process, the heat of the whole stack is mainly accumulated at the MgO layer due to its highest thermal resistance compared with the other layers. Previous work shows that the self-heating temperature of the whole device increases exponentially with the applied bias voltage [13]. In this work, the temperature increment of the overall device reaches up to 128 K with a voltage amplitude of 1.1 V. Fig. 3(a) shows the temperature distribution in the device during the heating process. Fig. 3(b) shows the temperature gradient on the MgO barrier during the cooling period, which is the main focus in the following research. The thermal conductivity difference between the MgO layer and the electrode is the main reason for the obvious temperature gradient in the barrier layer when the heat flux is transported from top to bottom. The temperature gradient at interface is of great significance to the study of the spin transport mechanism.

When the size of the device is shrank down into the nanometer scale, the thermal conductivity of the film is several orders of magnitude lower than the bulk value, which means that the existence of interfacial grain boundaries plays a non-negligible role in the interference of the heat transfer. The thermal conductivity of MgO κ_{MgO} used in the above study is the verified experimental value (4.8 W/m.K) [14]. Current studies show that the thermal conductivity of MgO thin films with a thickness of about 2 nm is between 0.4-4 W/m.K [15]. Furtherly, the temperature difference of the barrier layer of the MTJ device under different thermal conductivity parameters in the working state is compared by numerical simulation.

Fig. 4 visually shows the temperature difference between different layers of the MTJ device with varying κ_{MgO} values by fixing the temperature of the bottom electrode. When the thermal conductivity decreases by an order of magnitude, the temperature difference across the stack increases dramatically. The main temperature difference distribution is intensively manifested in the barrier layer. The results in Fig.4 illustrate the temperature difference across the MgO barrier with varying thermal conductivity values.

Fig. 5(a) shows the temperature difference under different thermal conductivity values. It can be observed a second power relationship between the temperature difference and the applied voltage in both the P state and the AP state. The increments in the applied bias voltage intensify the effect of thermal conductivity on ΔT across the MgO layer. In addition, the growth coefficient A fitted according to the second power relationship between bias voltage and ΔT across the MgO as a function of κ_{MgO} is shown in Fig. 5(b), highlighting the dominant effect of thermal conductivity parameters on the temperature gradient.

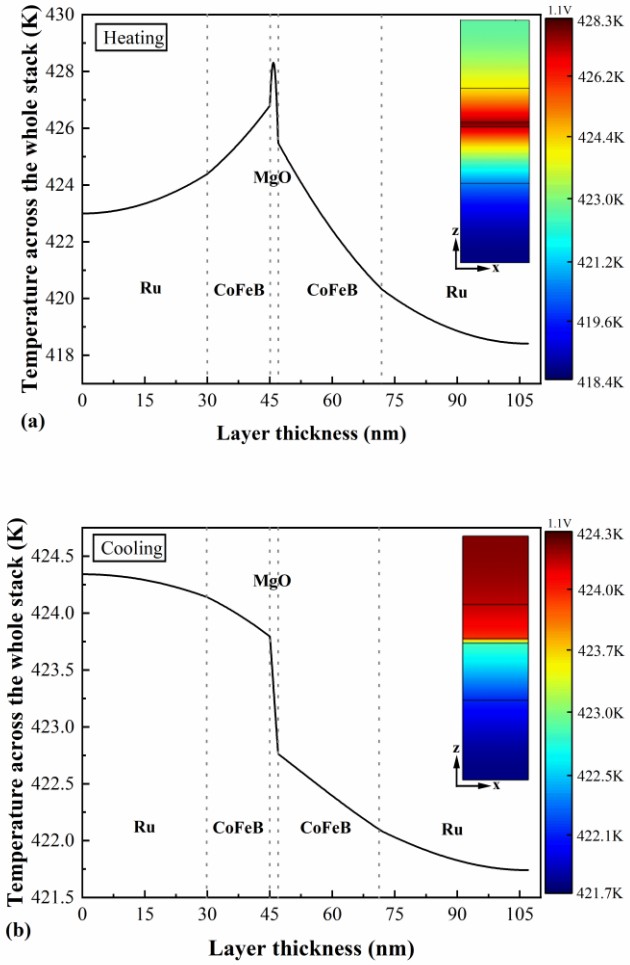

Fig. 3. (a) The temperature profile in the MTJ device at 2 ns under the heating process. (b) The temperature gradient on the stack at 2.05 ns under the cooling process. The ambient temperature is set to be 300 K and the applied pulse amplitude is 1.1 V.

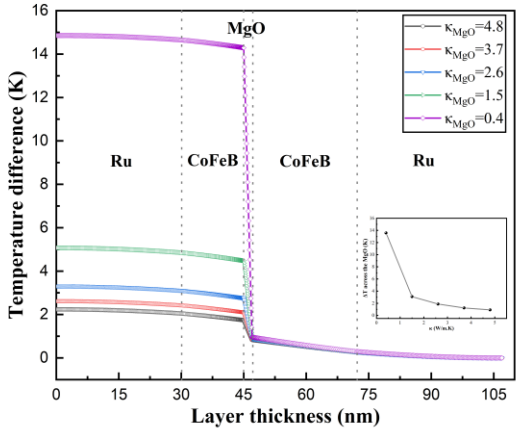

Fig. 4. The temperature difference profile across the MTJ device with varying κ_{MgO} values. The illustration refines the variation of the temperature difference across the MgO layer with κ_{MgO}.

This article has been accepted for publication in a future issue of this journal, but has not been fully edited. Content may change prior to final publication. Citation information: DOI 10.1109/TMAG.2022.3153363, IEEE Transactions on Magnetics

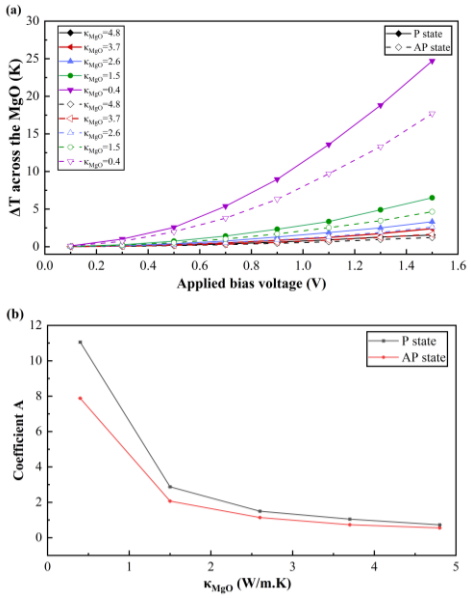

Fig. 5. (a) ΔT across the MgO as function of applied bias voltage under different κ_{MgO} values in P state and AP state. (b) The relationship between thermal conductivity and the growth coefficient A, which is extracted from the fitting data according to the second power relationship between bias voltage and ΔT across the MgO.

B. The mechanism of the phonon-electron coupling on heating transport

The imbalance in the transportation of the electron and the phonon at the metal-oxide interface causes an imbalance distribution of the electron and the phonon in the metal near the interface, resulting in additional thermal resistance. The thermal conductivity of the nanomagnetic interface materials is extremely sensitive to the imbalance of the electron and the phonon temperature in the spintronic device. It is the imbalance of the electron and the phonon that mainly accounts for the effect of the thermal conductivity on temperature gradient.

To explore the contribution of the phonon and the electron to the thermal transportation, the entire heat transfer system is divided into two parts: the electron part and the phonon part. The temperature of the electronic system (T_e) is mainly contributed by the electron on the CoFeB side, and the phonon system is mainly determined by the phonon temperature (T_p) on the CoFeB and the MgO side. The coupling equation of the electron and the phonon subsystem on the metal side is solved with the preliminary assumption that the Fourier law is valid in the system. The metal side heat transfer along the x-axis satisfies the energy conservation equation:

$$\kappa_e^M \frac{d^2T_e(x)}{dx^2} - G_{ep}[T_e(x) - T_p(x)] = 0 \quad (2a)$$

$$\kappa_p^M \frac{d^2T_p(x)}{dx^2} + G_{ep}[T_e(x) - T_p(x)] = 0 \quad (2b)$$

where κ_e^M and κ_p^M are the electronic thermal conductivity and phonon thermal conductivity of CoFeB material, respectively. G_{ep} is the phonon-electron interface coupling factor.

Subtracting the above two equations, we get

$$\frac{d^2\theta}{dx^2} - \frac{\theta}{\delta^2} = 0 \quad (3)$$

where $\theta = T_e - T_p$ and

$$\frac{1}{\delta^2} = \frac{1}{\delta_e^2} + \frac{1}{\delta_p^2} \quad (4)$$

where δ the characteristic length of electron-phonon imbalance and $\delta_i^2 = \kappa_i^M / G_{ep}$, i the subscript notation of the phonon and the electron. Given that the energies of the electron and the phonon is conserved away from the interface, the boundary conditions satisfy $\theta|_{x\to\infty} = 0$.

By solving (2a) and (2b), the temperature distribution of the electron and the phonon can be obtained:

$$T_e^{L(R)}(x) = +(-)A_1 \exp(x/\chi) + B_1 x + C_1 \quad (5a)$$

$$T_p^{L(R)}(x) = +(-)A_2 \exp(x/\chi) + B_2 x + C_2 \quad (5b)$$

Where L and R represent the boundary of CoFeB on both sides, and the length is defined as 10 nm. A_1, A_2, B_1, B_2, C_1, C_2 are the unknown coefficients.

The Dirichlet boundary conditions at the interfaces are defined as:

$$\begin{aligned}
&\kappa_e^M \left.\frac{dT_e^L(x)}{dx}\right|_{x=-d} = \kappa_e^M \left.\frac{dT_e^R(x)}{dx}\right|_{x=d} = 0 \\
&\kappa_p^M \left.\frac{dT_p^L(x)}{dx}\right|_{x=-d} = \kappa_p^M \left.\frac{dT_p^R(x)}{dx}\right|_{x=d} \\
&\kappa_{MgO}[T_{e(p)}^L(-d) - T_{e(p)}^R(d)] = -\kappa_{e(p)}^M \left.\frac{dT_{e(p)}^R(x)}{dx}\right|_{x=d} \\
&T_{e(p)}^L(x=L) = 302K,\ T_{e(p)}^R(x=R) = 300K
\end{aligned} \quad (6)$$

Fixing the temperatures on both sides of the metal, the temperature distribution of the electron and phonon subsystems including interfaces of CoFeB/MgO/CoFeB structure is characterized, as shown in Fig. 6. The parameters for the calculation are listed in TABLE II. The κ_e and κ_p of CoFeB are approximately equal to the first-principles prediction of Co. [16], indicating that κ_p accounts for 14.18% of κ_{total}, where $\kappa_{total} = \kappa_e + \kappa_p$.

At the boundary, the imbalance effect of the electron and the phonon is revealed, which is intensified with κ_{MgO} increasing. The defined effective temperature is used to describe the temperature gradient of the whole system. With the decreasing of κ_{MgO}, the effective temperature difference ΔT_{eff} including the phonon-electron coupling is elevated, consisting with the results simulated by FEM. The phonon-electron imbalance effect at the interface is the main cause of the temperature gradient and the selected thermal conductivity coefficient determines the effective temperature difference of the whole nanodevice.

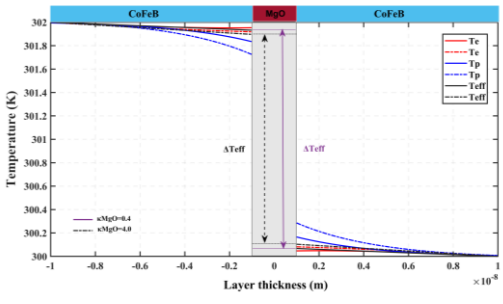

Fig. 6. The temperature distribution of the system including the electron

temperature (T_e), phonon temperature (T_p) and effective temperature (T_{eff}) when the κ_{MgO} is 0.4 and 4 W/m.K, respectively. The black dotted line and purple solid line mark the effective temperature difference at different κ_{MgO}.

TABLE II
KEY PARAMETERS FOR CALCULATION

κ_e(W/(m.K))	κ_p (W/(m.K))	κ_{MgO}(W/(m.K))	G_{ep}(W/(m^3.K))
75.52	12.48	0.4/4	9.93e17

C. Improved heat transportation model adjusted by parameterization

At the interface of CoFeB and MgO, the heat flow is mainly transferred by phonon. However, when the size of the device is reduced down to the nanoscale, the coupling effect of the electron and the phonon cannot be ignored because of the increasing collision frequency caused by the boundary scattering. Fig. 6 shows that the phonon-phonon temperature difference is less than the ΔT_{eff} of the whole system including the phonon-electron coupling, which is also the main reason why the previously simulated temperature difference system is less than the experimental measured temperature difference. Furtherly, it is necessary to optimize the heat transport model by parameterizing the interface phonon-electron coupling information, which can improve the accuracy of the model.

The interface area is re-planned and located on metal side. The quantified phonon-electron imbalance distance is estimated as:

$$\delta_1 = \sqrt{\frac{1}{G_{ep}} \frac{\kappa_e^M \kappa_p^M}{\kappa_e^M + \kappa_p^M}} \tag{7a}$$

$$\delta_2 \approx 1.2\delta_1 = 1.2\sqrt{\frac{1}{G_{ep}} \frac{\kappa_e^M \kappa_p^M}{\kappa_e^M + \kappa_p^M}} \tag{7b}$$

where δ_1 and δ_2 are imbalance distance when κ_{MgO} is equal to be 0.4 and 4 W/m.K, respectively.

The thermal resistance at the interface is defined as:

$$R_{interface} = R_{ep} + R_{pp} \tag{8}$$

where R_{ep} the thermal resistance due to phonon-electron coupling on the metal side and R_{pp} the thermal resistance caused by heat flow through the CoFeB/MgO interface.

Therefore, the thermal conductivity of the interface can be obtained:

$$\kappa_{interface} = \frac{1}{R_{ep}+R_{pp}} = \frac{\kappa_{ep}\kappa_{pp}}{\kappa_{ep}+\kappa_{pp}} \tag{9}$$

where κ_{ep} and κ_{pp} are the reciprocals of R_{ep} and R_{pp}, corresponding to the thermal conductivity values of the corresponding channels, respectively. The κ_{ep} emphasized in the improved model can be estimated by the coupling coefficient, $\kappa_{ep} = \sqrt{G_{ep}\kappa_p^M}$.

Fig. 7(a) shows the improved model structure. The increased phonon-electron imbalance distance is located on the metal side of the CoFeB/MgO interface. Fig. 7(b) displays the temperature profile of the two models including the information of the interface thickness (δ_1 =3.28 nm, δ_2 =3.94 nm). It can be seen that the temperature gradient of the improved model is elevated compared to initial model regardless of whether the conductivity is 0.4 or 4 W/m.K. This method of parametric improvement of the model is taken into account by the phonon-electron coupling, which makes up for the limitations of traditional method via FEM simulation.

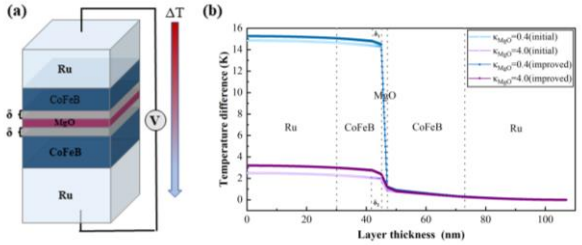

Fig. 7. (a) The improved model structure including quantified phonon-electron imbalance distance. (b) Comparison of normalized temperature distribution between improved model and initial model.

The parameterization method is used to add interface information to the finite element model so that the temperature gradient displayed by the improved model better reflects the temperature difference of the film layer interfaces. This method can effectively simulate the heat transportation of thin film stack devices.

It is worth noting that this temperature gradient is very important for studying the interface charge transport mechanism [17] and the TMS effect of thermovoltage devices [18]. At the same time, considering the influence of materials and bias on the interface effect is also valuable for the reliable research of the device, which means that an effective model has important guiding significance for the following work.

IV. CONCLUSION

The self-heating and stack temperature profile distribution of the MTJ device under the working state is described by heat transfer model established via FEM. For nano-scale MTJ device, the temperature gradient across the whole stack is extremely sensitive to the thermal conductivity parameters of the oxide layer. When the κ_{MgO} is decreased by an order of magnitude, the device interface temperature difference is increased exponentially. The increased bias voltage exacerbates the temperature difference both in P state and AP state. Furthermore, the heat transfer mechanism is implemented to characterize the non-equilibrium heat transfer phenomenon of the phonon and the electron subsystems. The increment in thermal conductivity aggravates the phonon and electron imbalance effect. The defined effective temperature difference accounts for the effect of thermal conductivity on the temperature difference. Moreover, the improved model established by quantifying the phonon-electron non-equilibrium distance δ and the interface thermal conductivity κ_{inter} effectively compensates for the traditionally established limit that the temperature difference is lower than the experimental value, making the obtained temperature distribution within the MTJ closer to the actual. This method provides guidance for the obtained temperature distribution in the MTJ device under the working state.

REFERENCES

[1] N. Perrissin1, S. Lequeux, and N. Strelkov, "Highly thermally stable sub-20nm magnetic random-access memory based on perpendicular shape anisotropy," *Nanoscale*, vol. 10, pp. 12187-12195, 2018.

[2] L. Y. Zhang, Y. Q. Cheng, and Y. G. Zhang, "Addressing the thermal issues of STT-MRAM from compact modeling to design techniques," *IEEE Transactions on nanotechnology*, vol. 17, pp. 345-352, 2018.

[3] R. Okuno, Y. Yamada, and M. Goto, "Enhanced electric control of magnetic anisotropy via high thermal resistance capping layers in magnetic tunnel junctions," *Journal of Physics: Condensed Matter*, vol. 32, pp. 384001, 2020.

[4] T. Kuschel, M. Czerner, and J. Walowski, "Tunnel magneto-Seebeck effect," *Journal of Physics D: Applied Physics*, pp. 1-19, 2018.

[5] Z. H. Zhang, L. H. Bai, and X. B. Chen, "Observation of thermal spin-transfer torque via ferromagnetic resonance in magnetic tunnel junctions," *Physical Review B*, vol. 94, pp. 064414, 2016.

[6] K. Kim, C. Choi, and Y. Oh, "Time-dependent dielectric breakdown of MgO magnetic tunnel junctions and novel test method," *Jpn. j. appl. phys*, vol. 56, pp. 04CN02, 2017.

[7] B. Shi, "Interfacial thermal conductance at metal-nonmetal interface via electron-phonon coupling," *Modern Physics Letters B*, vol. 32, pp. 1830004, 2018.

[8] T. Huebner, U. Martens, and J. Walowski, "Thermal conductivity of thin insulating films determined by tunnel magneto-Seebeck effect measurements and finite-element modeling," *J. Phys. D: Appl. Phys*, vol. 51, pp. 224006, 2018.

[9] M. J. Li, Y. Y. Wang, and J. Zhou, "Thermal boundary conductance across metal-nonmetal interfaces: effects of electron-phonon coupling both in metal and at interface," *The European Physical Journal B*, vol. 88, pp.1-7, 2015.

[10] D. Austin, M. Sadid, and A. Mustafa, "Analysis of self-heating of thermally assisted spin-transfer torque magnetic random access memory," *Beilstein Journal of Nanotechnology*, vol. 7, pp. 1676–1683, 2016.

[11] H. Cansever, J. Lindner, and T. Huebner, "Characterization of continuous wave laser-induced thermal gradients in magnetic tunnel junctions integrated into microresonators via COMSOL simulations," *IEEE Transactions on magnetics*, vol. 55, pp. 1-5, 2019.

[12] B. Teso, A. Siritaratiwat, and C. Surawanitkun, "Different Effect of Temperature Increment on CoFeB/MgO Based Single and Double Barrier Magnetic Tunnel Junctions during Switching Process in STT-MRAM," in *2018 15th International Conference on Electrical Engineering/Electronics, Computer, Telecommunications and Information Technology (ECTI-CON)*, 2018.

[13] X. Zhang, G. J. Zhang, and L. J. Shen, "Life-time degradation of STT-MRAM by self-heating effect with TDDB model," *Solid State Electronics*, vol. 173, pp. 107878, 2020.

[14] H. J. Jang, L. Marnitz, and T. Huebner, "Thermal conductivity of oxide tunnel barriers in magnetic tunnel junctions measured by ultrafast thermoreflectance and magneto-optic kerr effect thermometry," *Physical Review Applied*, vol. 13, pp. 024007, 2020.

[15] T. Huebner, U. Martens, and J. Walowski, "Thermal conductivity of thin insulating films determined by tunnel magneto-Seebeck effect measurements and finite-element modeling," *Journal of Physics D Applied Physics*, vol. 51, pp. 224006, 2018.

[16] Z. Tong, S. H. Li, and X. L. Ruan, "Comprehensive first-principles analysis of phonon thermal conductivity and electron-phonon coupling in different metals," *Physical Review B*, vol. 100, pp. 144306, 2019.

[17] V. Popescu, P. Kratzer, and P. Entel, "Spin caloric transport from density-functional theory," *Journal of Physics D Applied Physics.* Vol. 52, pp. 073001, 2019.

[18] S. Jain, D. D. Lam, and A. Bose, "Magneto-Seebeck effect in spin-valve with in-plane thermal gradient," *AIP Advance.* Vol. 4, pp. 127145. 2014.